Supplementary Information for

Large-Scale Computational Screening of Binary Intermetallics for Membrane-based Hydrogen Separation

Nita Chandrasekhar[a,b], David S. Sholl[a,*]

[a] *School of Chemical & Biomolecular Engineering, Georgia Institute of Technology, Atlanta, Georgia, USA 30332*

[b] *Current address: Praxair, Inc. 175 East Park Dr., Tonawanda, NY 14209*

**Corresponding author. Email: david.sholl@chbe.gatech.edu*

1. Overview of method

The following figure illustrates the algorithm of the method developed in this work to screen hundreds of intermetallic structures without compromising on the accuracy of our predictions.

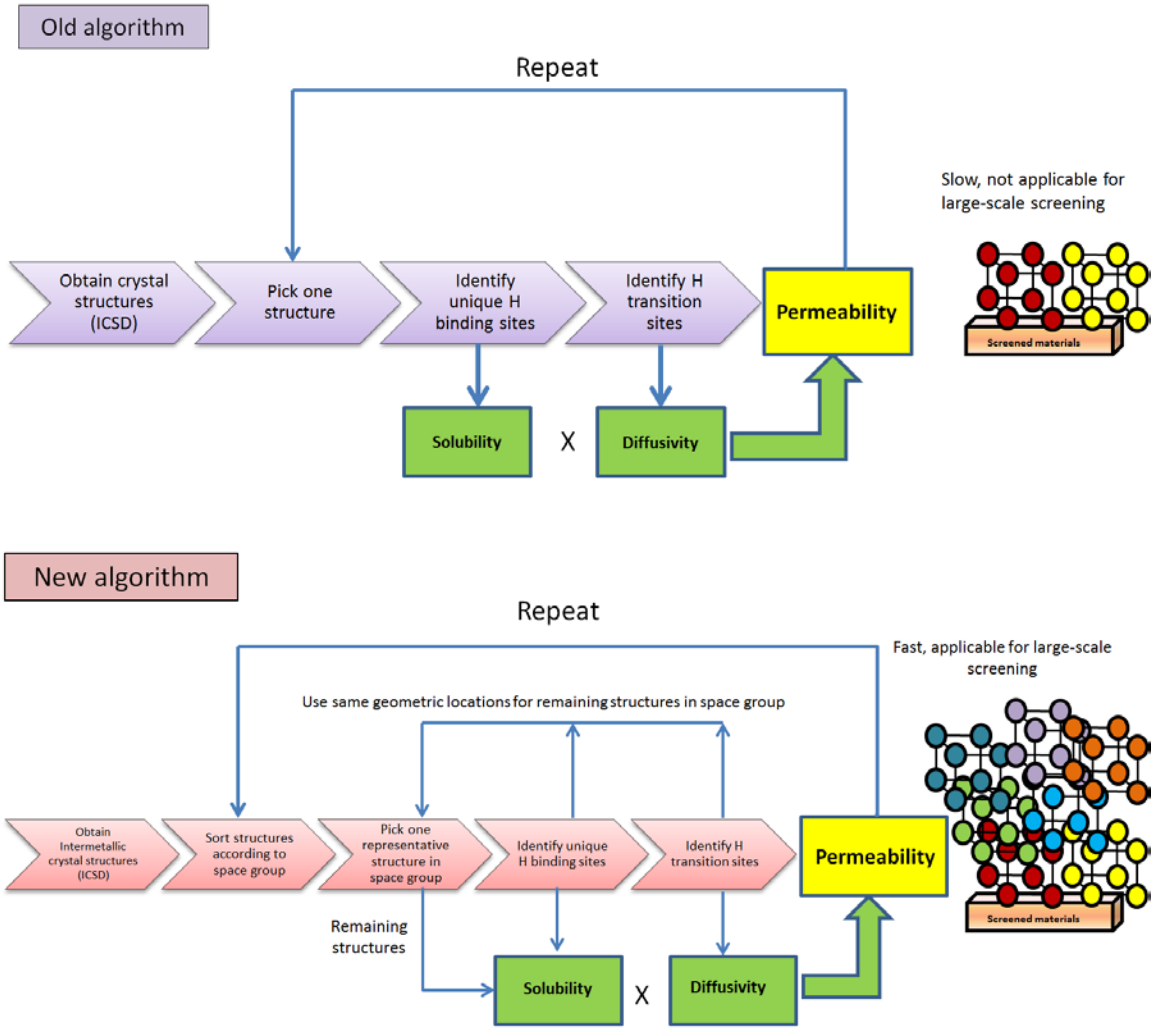

Figure S1: A schematic comparison of the old method[1] and the new algorithm developed to rapidly screen favorable materials for H separation from 981 binary intermetallics. This method exploits the geometries of the different structures to

reduce the total number of DFT calculations needed to evaluate properties enabling the screening of orders of magnitude more materials than possible previously. This method is easily automated using python libraries such as PYMATGEN and is more efficient than previous methods of computational prediction.

2. Screening Algorithm for non-Pd based intermetallics

In the main text, the screening process for identifying non-Pd based membranes from ICSD[2]. In this section, the selection process for identifying suitable H membrane materials from thousands of intermetallics listed in ICSD is explained in detail. A search in the ICSD for binary intermetallics that are a combination of alkali and alkaline earth metals, all d-block metals and Al, Ga, In, Sn, Tl, Pb and Bi from the p-block lists 1625 unique materials. Structures for which no specific melting temperatures or pressures were provided in ICSD were also included in this study. When multiple entries existed for the same material that listed identical crystal structures and lattice constants, the most recent entry was used for further analysis.

From these entries, the materials unsuitable for membrane applications due to various factors were removed. The different criteria used to remove materials and the number of such entries removed from the list of candidates is listed in Table S1.

Table S1: List of the various conditions used to sort the candidate materials. The number of materials satisfying each condition is listed on the right.

Condition	No.
All ICSD entries	1625
Materials with multiple phases	127
Materials with $T_{melt} < 1500$ K	104
Materials stable only at high pressures (> 10 atm)	15
Materials stable only above 500 K	89
Purely computational structures	35
Remaining candidates	**1255**

There are 127 materials that show multiple phases i.e. undergo a phase transition at some temperature from 400-1200 K. For example, the intermetallic NiPt undergoes a change in structure from P4/mmm to Fm-3m at 1000 K. For these materials the individual phases were treated as separate materials at the conditions specified. For example, at temperatures < 1000 K, the calculations to predict solubility of NiPt were performed on its P4/mmm structure, while the Fm-3m structure was used at temperatures > 1000 K. The H solubility of each of the phases of the 127 materials was calculated individually for the relevant temperature ranges. These materials were

included in the analysis of potential candidate materials and a total of 1382 materials (1255+127) were screening using the method described in the main text.

Materials that are stable only at high temperatures (> 500 K) or high pressures (> 10 atm) were removed from the list. Many intermetallics had melting points < 1500 K. For membrane purposes, thermal stability at high temperatures is essential since gas streams containing a mixture of hydrogen and other gases can be produced at 1093 K or higher temperatures[3] . Hence materials with melting points (T_{melt}) lower than 1500 K were removed from the list of potential candidates.

We did not include intermetallic phases whose existence was reported purely computationally. It is possible that other intermetallic structures exist that have not yet been discovered or reported in the ICSD. Their identification however, is beyond the scope of this work.

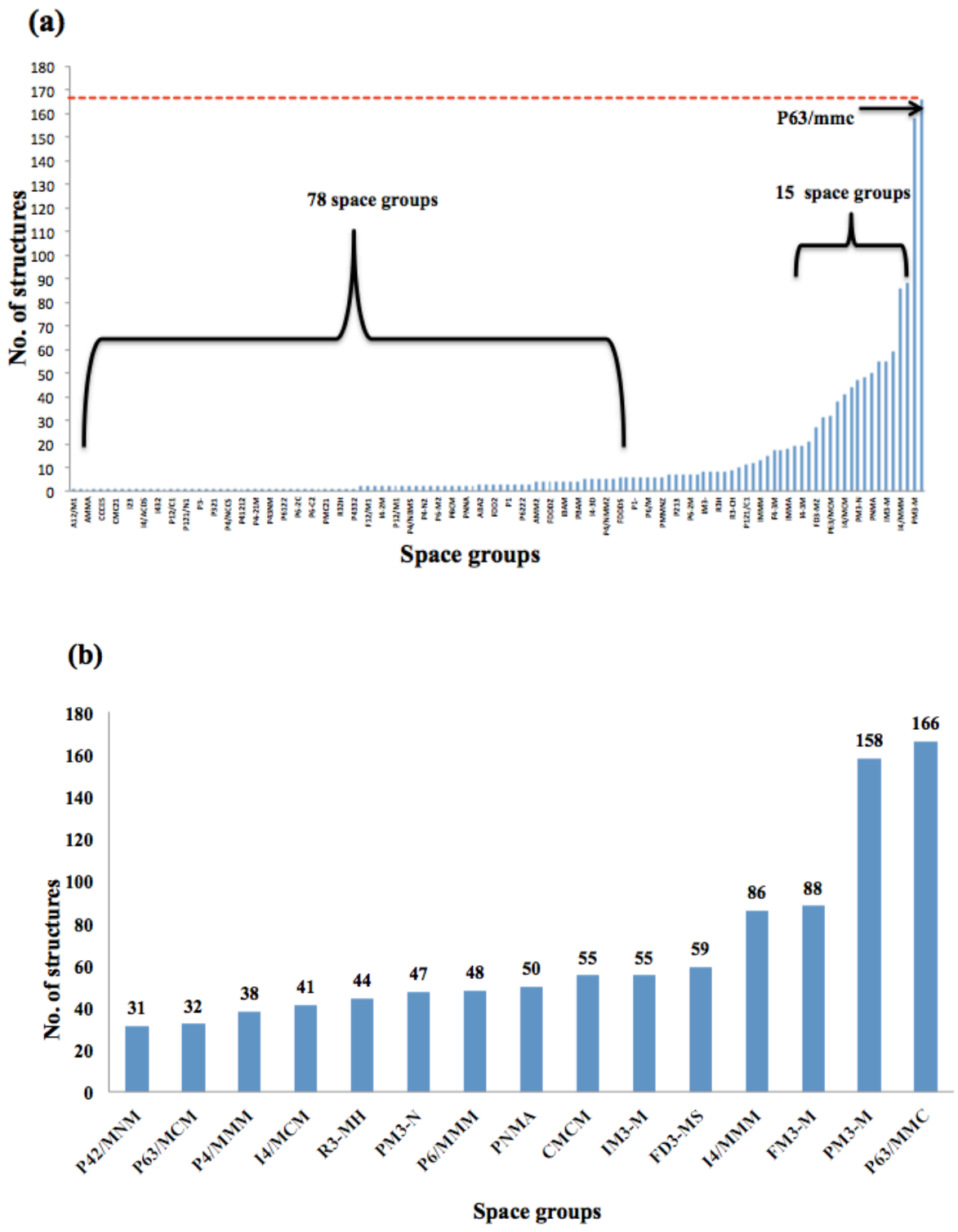

Figure S2: (a) 1255 intermetallic materials sorted into 123 space groups. The horizontal axis represents the space groups and the vertical axis is the number of materials in each space group. 78 space groups having 5 materials or less are

highlighted. P63/mmc is the space group with the maximum number of materials (166), shown by the red dashed line. For reasons of clarity, not all space groups are labeled on the horizontal axis. (b) The top 15 most populated space groups considered in this work.

From Fig. S2, we can observe that there are some space groups such as P63/mmc that have a large number of candidate structures (166) and there are 78 space groups that have 5 or less candidate structures. To make the screening process efficient, the space groups were ranked based on the number of candidate structures of each type in the space group and the top 15 were selected for the next steps in the screening process. A substantial proportion of structures (64%) belong to these 15 groups. These 15 space groups include 981 materials that meet the other criteria listed in Table S1.

To rapidly identify favorable candidates from the 981 materials in 15 space groups using solubility as a screening parameter and a minimum number of DFT calculations, a representative structure was chosen randomly from each space group. The top 15 space groups and the representative material chosen for each space group are shown in Table S2. The total number of structures that belong to the 15 space groups is 995. This includes 14 materials that show two phases where both phases belong to the 15 space groups. This results in 981 unique materials (removing the double counted materials). In the case of Cu_3Sn, one of the structures belongs to the top 15 space groups (P63/mmc) however the other low temperature structure belongs to F4-3m space group which is not one of the 15 space groups. Similarly HfV_2 has two other low temperature phases (Fd-3mz and Imma) apart from Fd-3ms, which are not included in these 15 space groups. NiTi shows three other structures apart from its Pm-3m structure i.e. P-, P121/m1 and P1121/m. For these three materials the 6 structures that do not belong to the 15 most populated space groups were also considered and the calculations were performed separately for the relevant temperatures. In total, in this work, calculations were performed on 1001 (995+6) structures.

During the solubility calculation using the method described in the main text unique H binding sites in each material are identified. We simplified our analysis by assuming that the geometry of these unique binding sites is common between crystal structures within the same space group. This assumption is consistent with data from previous calculations for different Fm-3m (fcc) structures that resulted in consistent geometric locations of the H-binding sites[4,5]. Although the locations of binding sites are the same in similar materials, the binding energy of H in each material depends on the material's constituent elements.

Table S2: The top 15 most common space groups along with the number of structures of each space group type are shown. The prototype column lists the composition of the intermetallic selected as the representative structure of the space group.

Rank	Space Group	No. of structures	Representative Structure
1	P63/mmc	166	Fe_2Nb_1
2	Pm-3m	158	Co_1Ti_1
3	Fm-3m	88	Ir_1Sn_2
4	I4/mcm	86	Ba_5Pb_3
5	Fd-3ms	57	Be_2Cu_1
6	Cmcm	55	Bi_2Ca_1
7	Im-3m	55	Nb_1Hf_1
8	Pnma	50	Au_1Y_2
9	P6/mmm	47	Fe_5Y_1
10	Pm-3n	47	Au_1Zn_3
11	R-3mh	44	Ir_3Y_1
12	I4/mmm	41	Au_2Hf_1
13	P4/mmm	38	Cd_3Zr_1
14	P63/mcm	32	Hf_5Ir_3
15	P42/mnm	31	Cr_2Ru_1

To ensure that DFT calculations give accurate lattice constants for the different materials considered, the lattice constants of the structures obtained from the ICSD[1] were compared with those obtained from DFT. The crystal structures obtained from the ICSD were used as input in geometric relaxation calculations performed using DFT. 169 of the candidate structures obtained from ICSD had partial occupancies or incomplete structures and could not be directly used as an input for DFT calculations. For these structures, the positions of the atoms were obtained from prototype structures and the lattice constants listed in the ICSD were used to construct a unit cell. For 158 structures, the resulting lattice parameters predicted by DFT calculations were in good agreement with the lattice constants listed in the ICSD. For the remaining 11 structures a difference in cell volume > 5% was found. These 11 structures are listed in Table S2 marked with an asterisk. In the remaining 832 structures whose structure files from the ICSD were directly used in DFT calculations, 25 structures had lattice constants that result in cell volumes that differ by greater than 5% from the values listed in ICSD. These 25 structures are listed in Table S3

(without the asterisk). For these structures, the DFT optimized structures were used for further calculations. The lattice constants calculated using DFT for the remaining 807 structures obtained directly from ICSD are in good agreement with the ICSD values. We used the DFT optimized structures for all materials as a starting point for the next steps in the screening process.

Material	ICSD values	ICSD volume	Calculated lattice parameters	DFT volume	DFT vol./ ICSD vol.
$InSn_4$	a=3.21,c= 3.00, α =β=90°,γ=120°	26.81	a=3.31,c= 3.56, α=β=90°,γ=120°	47.21	1.45
Pt_2Re_3*	a=2.77,c= 4.43,α=β=90°,γ=120°	29.32	a=2.96,c= 4.73,α=β=90°,γ=120°	46.16	1.41
NiRu	a=2.61, c=4.20, α=β=90°,γ=120°	24.70	a=2.74, c=4.6, α=β=90°,γ=120°	38.81	1.40
Ga_2Sr_1*	a=4.35,c= 4.74, α=β=90°,γ=120°	77.55	a=4.45,c= 5.15, α=β=90°,γ=120°	120.71	1.32
$Mg_{47}Pb_3$*	a=3.21,c=5.42, α=β=90°,γ=120°	46.86	a=3.26,c=5.58, α=β=90°,γ=120°	82.37	1.27
In_9Pb	a=3.27,c=5.03, α=β=γ=90°	53.82	a=3.57,c=5.25,α=β=γ=90°	66.95	1.24
CrFe*	a=2.9 ,α=β=γ=90°	24.39	a=3.1 ,α=β=γ=90°	29.79	1.22
Ti_7Zr_3*	a=3.03,c= 4.83, α=β=90°,γ=120°	38.40	a=3.05,c= 5.03, α=β=90°,γ=120°	46.80	1.22
IrPt*	a=3.88 ,α=β=γ=90°	58.28	a=4.12 ,α=β=γ=90°	90.52	1.20
CoV_3*	a=4.68 ,α=β=γ=90°	102.24	a=4.98 ,α=β=γ=90°	123.51	1.20
TaTi	a=3.29 ,α=β=γ=90°	35.48	a=3.49 ,α=β=γ=90°	59.32	1.19
Co_8Sn_{44}*	a=12.14 ,α=β=γ=90°	1787.11	a=12.84 ,α=β=γ=90°	2708.87	1.18
$Cr_{13}Ga_{13}$	a=12.63,c=7.79,α=β=90°,γ=120°	1074.61	a=12.75,c=7.89,α=β=90°,γ=120°	1269.24	1.18
Pt_3V_2*	a=3.86 ,α=β=γ=90°	57.56	a=4.05 ,α=β=γ=90°	91.13	1.16
Cu_4Ti_3	a=3.13,c=19.97,α=β=γ=90°	195.09	a=3.35,c=20.11,α=β=γ=90°	225.68	1.16
Ta_6Zn_7	a=5.04,c=27.53, α=β=90°,γ=120°	604.37	a=5.24,c=27.73,α=β=90°,γ=120°	697.87	1.15
$Be_{17}Zr_2$	a=7.54,c=11.02, α=β=90°,γ=120°	542.04	a=7.68,c=11.15,α=β=90°,γ=120°	625.89	1.15
$Mo_{17}Pt_3$*	a=4.89 ,α=β=γ=90°	124.18	a=5.20 ,α=β=γ=90°	191.10	1.13
$AuBe_{12}$	a=7.243,c=4.25, α=β=γ=90°	223.06	a=7.45,c=4.55,α=β=γ=90°	252.54	1.13
$CdLi_3$*	a=4.26 ,α=β=γ=90°	77.25	a=4.41 ,α=β=γ=90°	122.02	1.11
NbTa	a=3.3,α=β=γ=90°	35.94	a=3.42,α=β=γ=90°	54.87	1.11
Na_7Ga_{13}	a=15.63,b=14.98,c=21.7,α=β=γ=90°	5073.67	a=15.9,b=15.65,c=22.5,α=β=γ=90°	5598.79	1.10
Co_7Cr_8	a=b=8.81,c=4.56, α=β=γ=90°	353.93	a=b=8.91,c=4.86,α=β=γ=90°	385.83	1.09
Cs_4Sn_{23}	a=b=c=12.10,α=β=γ=90°	1769.80	a=b=c=12.43,α=β=γ=90°	1920.50	1.09

Material	ICSD values	ICSD volume	Calculated lattice parameters	DFT volume	DFT vol./ ICSD vol.
Ca_7Sn_6	a=7.87,b=23.81,c=8.465,α=β=γ=90°	1586.14	a=7.98,b=24.02,c=8.9,α=β=γ=90°	1705.81	1.08
$Fe_{23}Y_6$	a=b=c=12.08,α=β=γ=90°	1763.67	a=12.35,α=β=γ=90°	1883.65	1.07
$Sn_{10}Y_{11}$	a=11.53,c=16.91,α=β=γ=90°	2248.03	a=11.83,c=17.02,α=β=γ=90°	2381.93	1.06
Ba_5Pb_3	a=9.04,c=16.81, α=β=γ=90°	1374.23	a=9.24,c=17.09,α=β=γ=90°	1459.10	1.06
Nb_3Os_2	a=b=9.86,a=5.06, α=β=γ=90°	492.02	a=b=9.88,c=5.32, α=β=γ=90°	517.00	1.05
$Ba_{11}Bi_{10}$	a=b=13.21,c=19.37, α=β=γ=90°	3389.51	a=b=13.41,c=19.58,α=β=γ=90°	3565.77	1.05
Pb_4Sr_5	a=8.48,b=17.27,c=9.01, α=β=γ=90°	1319.51	a=8.58,b=17.47,c=9.07,α=β=γ=90°	1385.49	1.05

Table S3: Comparison of the experimental and the DFT calculated structural parameters of intermetallics for structures where there was > 5% deviation in cell volume from the reported ICSD structures. All distances are in Angstroms and volume in $Å^3$. The structures marked with an asterisk are the structures for which the structures were generated manually and not using the cif files from ICSD.

Table S4: List of intermetallic compounds and the energy of the most favorable H binding site. The solubility for these materials cannot be reliably calculated using Sieverts' law. These materials are not favorable for use as membranes.

Material	E_b (eV)	Material	E_b (eV)
Ti_7Zr_3	-4.78	Ga_2Y_3	-0.96
Ga_4Ti_6	-4.36	$Ga_{39}Na_{22}$	-0.92
$IrTi_3$	-4.03	Be_5Hf	-0.92
BiK_3	-3.56	Li_3Bi	-0.91
Ga_3Zr	-3.45	Ca_5Ga_3	-0.91
Ga_3Nb_5	-3.38	$CaGa_2$	-0.91
In_2Li_3	-2.8	GaLi	-0.91
$GaHf_2$	-2.77	$BaMg_2$	-0.9
$Bi_{10}Ca_{11}$	-2.7	CsRb	-0.89
MgIn	-2.6	Mg_2Sn	-0.87
Ga_3Hf_5	-2.56	Be_2Zr	-0.87
LiZn	-2.49	$Mg_{38}Sr_9$	-0.87
Ga_5Ni	-2.4	$Ga_{14}Li_3$	-0.86
$Bi_{10}Sr_{11}$	-2.3	CdLi	-0.86
Ga_4Nb_5	-1.93	$Ca_{11}Ga_7$	-0.85
Ga_3Ti_5	-1.86	$AuNa_2$	-0.84
$CaNi_2$	-1.78	Ga_3Hf_1	-0.81
$NaGa_4$	-1.75	Ga_3Sc_5	-0.78
$Mg_{23}Sr_6$	-1.7	$Ca_{13}Cd_{76}$	-0.76
$LiTl_1$	-1.65	Li_3Tl	-0.76
HfTi	-1.62	$CaMg_2$	-0.76
Ga_4Ti_5	-1.6	Ga_3Nb_2	-0.73
In_3Li_{13}	-1.6	Ga_2Li_3	-0.71
Ga_3Nb	-1.57	CaSr	-0.71
InNa	-1.57	$Ga_{10}Hf_{11}$	-0.67
$CdLi_3$	-1.56	TiZr	-0.67
$BaGa_4$	-1.56	K_8Sn_{46}	-0.65
Li_3Pd	-1.54	KPb_2	-0.65
Ga_3K_2	-1.54	Li_5Tl_2	-0.61
Li_2Sr_3	-1.5	$Na_{13}Pb_5$	-0.59
Sr_6Li_{23}	-1.46	HfSc	-0.57
$CaLi_2$	-1.35	Mg_2Pb	-0.56
$MgPd_3$	-1.34	$GaZr_2$	-0.56
Ga_4Sr	-1.34	$LiPt_2$	-0.54
$LiPt_7$	-1.2	$Ca_{31}Sn_{20}$	-0.52
$Be_{17}Hf_2$	-1.2	$BaLi_4$	-0.52
LiMg	-1.2	Mg_3In	-0.47
$GaTi_2$	-1.2	$BiSr_2$	-0.47
MgSc	-1.07	Ba_6Mg_{23}	-0.45
Ga_5Mg_2	-1.04	$Ba_{10}Ga$	-0.42
Be_2Hf	-1.04	Ag_3Ca_5	-0.38
MgRh	-1.04	Cs_6K_7	-0.37
Ga_7Li_2	-1.03	NaTl	-0.35

HfOs	-1.03	$BiCa_2$	-0.33
GaY	-1.03	Au_2Na	-0.33
$LiPd_7$	-0.98	In_4K	-0.3

3. Solubility as a screening parameter

As described in the main text, solubility was used as a screening parameter to identify suitable intermetallic membrane materials for H separation. The solubility based screening was showing for Cmcm space group as an example in the main text. The remaining 14 space groups are shown below.
The diffusion activation energy of the shortlisted materials from each of the space groups using the solubility as a screening parameter is shown in table S5.

Figure S3: Solubility (H/M) of hydrogen at 600 K and 1 atm H_2 in intermetallics belonging to a specific space group. Each data point is labeled by the respective intermetallic. The solubility (H/M) for pure Pd computed with the same methods is shown as a horizontal solid line for comparison. The volume/metal atom for pure Pd is 15.9 Å^3. The black solid line and the red dashed line show the favorable solubility range used to screen candidates (10^{-1}-10^{-5} H/M). Intermetallics belonging to 14 space groups are shown here, with the identity of the space group indicated on each figure.

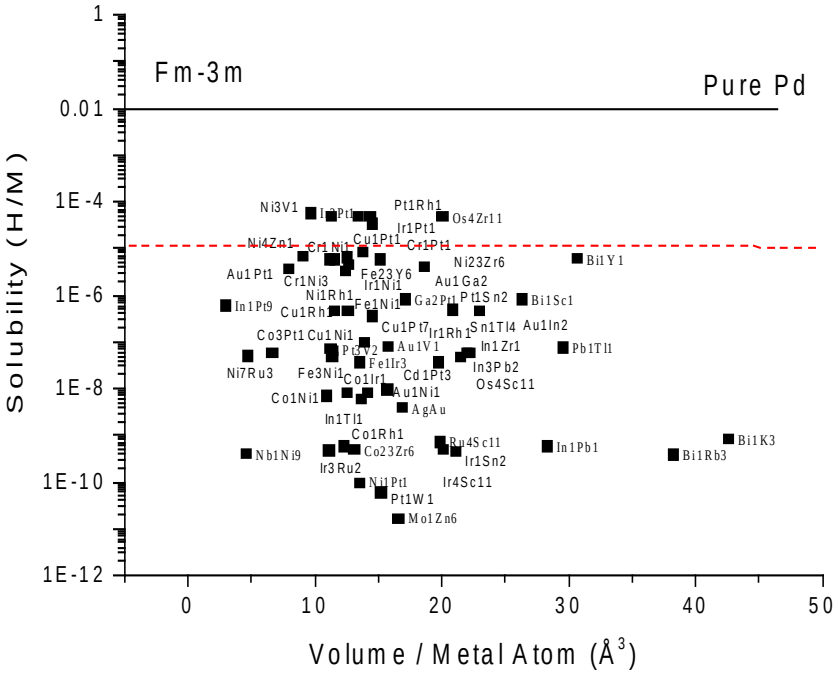

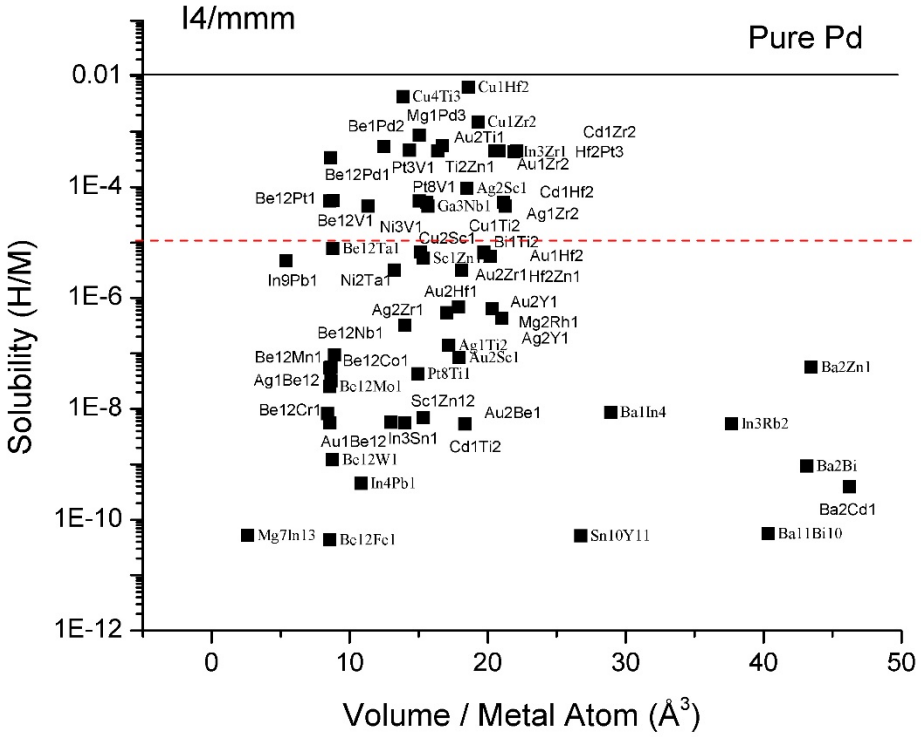
I4/mmm
Pure Pd
Solubility (H/M)
Volume / Metal Atom (Å3)
0.01
1E-4
1E-6
1E-8
1E-10
1E-12
0
10
20
30
40
50
Cu4Ti3
Cu1Hf2
Mg1Pd3
Be1Pd2
Cu1Zr2
Au2Ti1
Cd1Zr2
In3Zr1
Hf2Pt3
Be12Pd1
Pt3V1
Ti2Zn1
Au1Zr2
Pt8V1
Ag2Sc1
Cd1Hf2
Be12Pt1
Ga3Nb1
Ag1Zr2
Be12V1
Ni3V1
Cu1Ti2
Cu2Sc1
Bi1Ti2
Be12Ta1
Sc1Zn1
Au1Hf2
In9Pb1
Ni2Ta1
Au2Zr1
Hf2Zn1
Au2Hf1
Ag2Zr1
Au2Y1
Mg2Rh1
Be12Nb1
Ag2Y1
Ag1Ti2
Be12Mn1
Be12Co1
Au2Sc1
Ba2Zn1
Ag1Be12
Be12Mo1
Pt8Ti1
Sc1Zn12
Be12Cr1
Au2Be1
Ba1In4
In3Rb2
Au1Be12
In3Sn1
Cd1Ti2
Be12W1
Ba2Bi
In4Pb1
Ba2Cd1
Mg7In13
Be12Fe1
Sn10Y11
Ba11Bi10

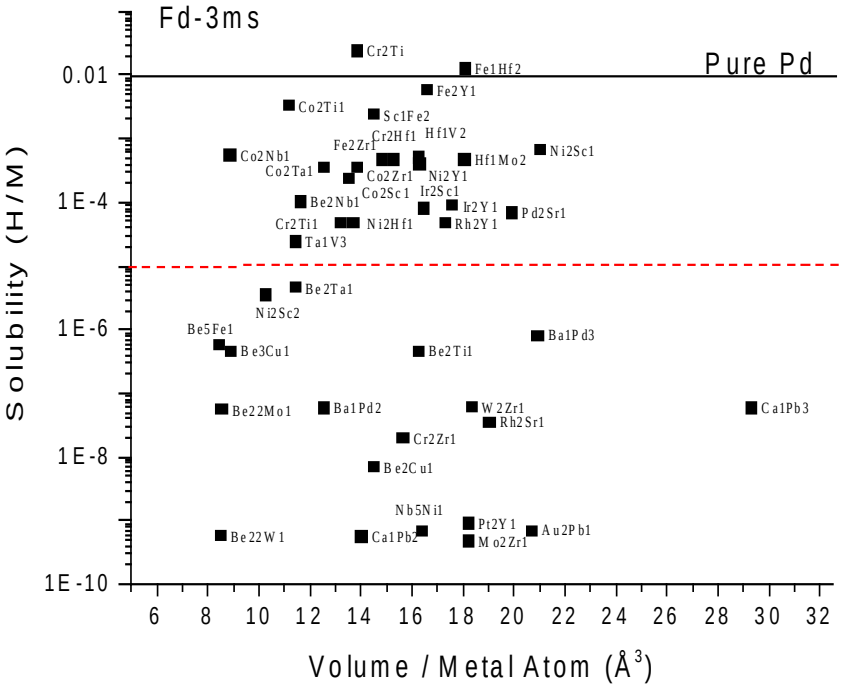
Fd-3ms
Pure Pd
Solubility (H/M)
Volume / Metal Atom (Å3)
0.01
1E-4
1E-6
1E-8
1E-10
6
8
10
12
14
16
18
20
22
24
26
28
30
32
Cr2Ti
Fe1Hf2
Fe2Y1
Co2Ti1
Sc1Fe2
Cr2Hf1
Hf1V2
Fe2Zr1
Co2Nb1
Ni2Sc1
Co2Ta1
Hf1Mo2
Co2Zr1
Ni2Y1
Co2Sc1
Ir2Sc1
Be2Nb1
Ir2Y1
Pd2Sr1
Cr2Ti1
Ni2Hf1
Rh2Y1
Ta1V3
Be2Ta1
Ni2Sc2
Be5Fe1
Ba1Pd3
Be3Cu1
Be2Ti1
Be22Mo1
Ba1Pd2
W2Zr1
Ca1Pb3
Rh2Sr1
Cr2Zr1
Be2Cu1
Nb5Ni1
Pt2Y1
Au2Pb1
Be22W1
Ca1Pb2
Mo2Zr1

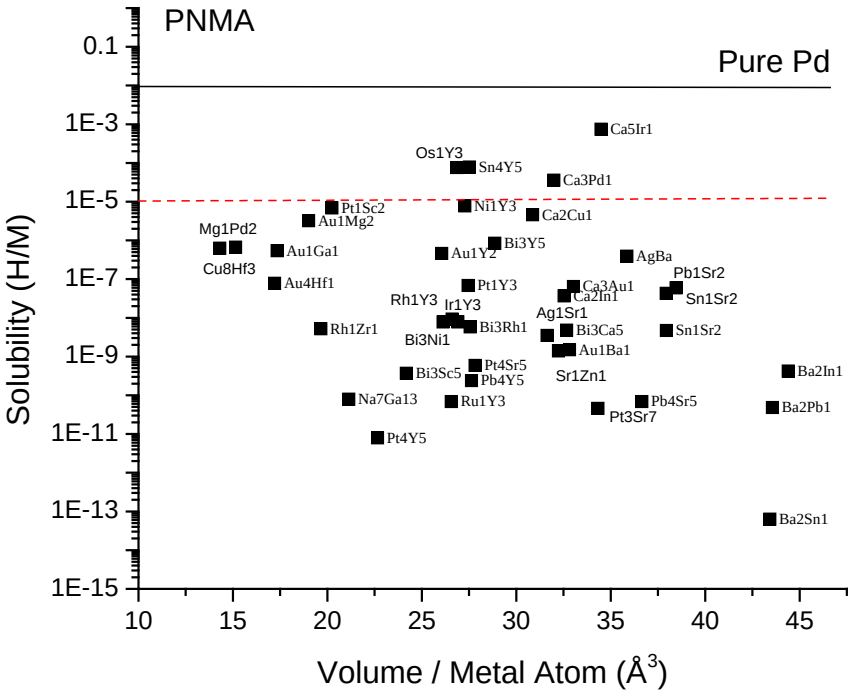
PNMA
Pure Pd
Solubility (H/M)
Volume / Metal Atom (Å3)
0.1
1E-3
1E-5
1E-7
1E-9
1E-11
1E-13
1E-15
10
15
20
25
30
35
40
45
Ca5Ir1
Os1Y3
Sn4Y5
Ca3Pd1
Pt1Sc2
Ni1Y3
Ca2Cu1
Au1Mg2
Mg1Pd2
Au1Ga1
Bi3Y5
Au1Y2
AgBa
Cu8Hf3
Au4Hf1
Pt1Y3
Ca3Au1
Pb1Sr2
Ca2In1
Sn1Sr2
Rh1Y3
Ir1Y3
Ag1Sr1
Rh1Zr1
Bi3Rh1
Bi3Ca5
Sn1Sr2
Bi3Ni1
Au1Ba1
Pt4Sr5
Sr1Zn1
Ba2In1
Bi3Sc5
Pb4Y5
Na7Ga13
Ru1Y3
Pb4Sr5
Ba2Pb1
Pt3Sr7
Pt4Y5
Ba2Sn1

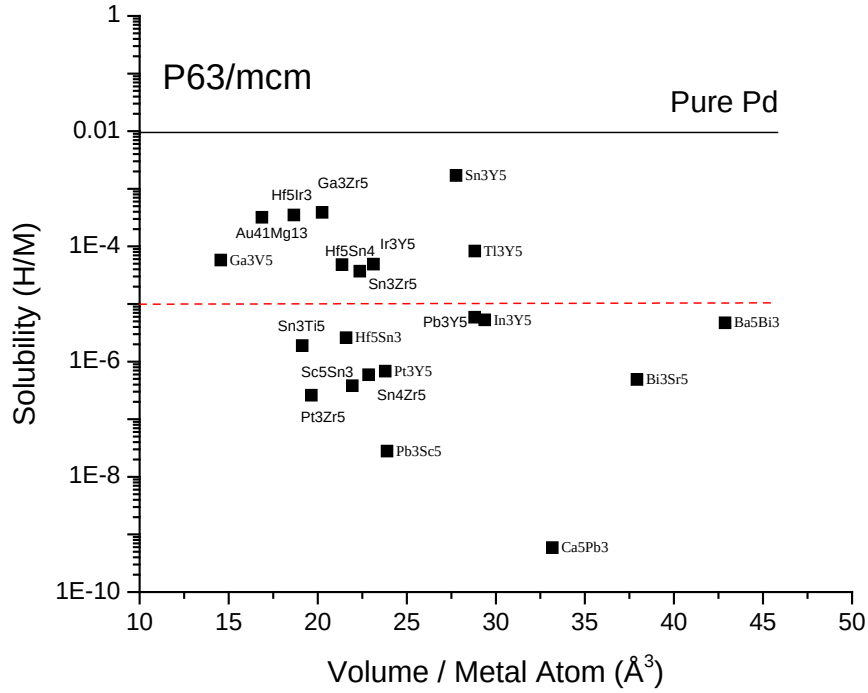
P63/mcm
Pure Pd
Solubility (H/M)
Volume / Metal Atom (Å3)
1
0.01
1E-4
1E-6
1E-8
1E-10
10
15
20
25
30
35
40
45
50
Sn3Y5
Ga3Zr5
Hf5Ir3
Au41Mg13
Ga3V5
Hf5Sn4
Ir3Y5
Tl3Y5
Sn3Zr5
Sn3Ti5
Pb3Y5
In3Y5
Ba5Bi3
Hf5Sn3
Sc5Sn3
Pt3Y5
Bi3Sr5
Sn4Zr5
Pt3Zr5
Pb3Sc5
Ca5Pb3

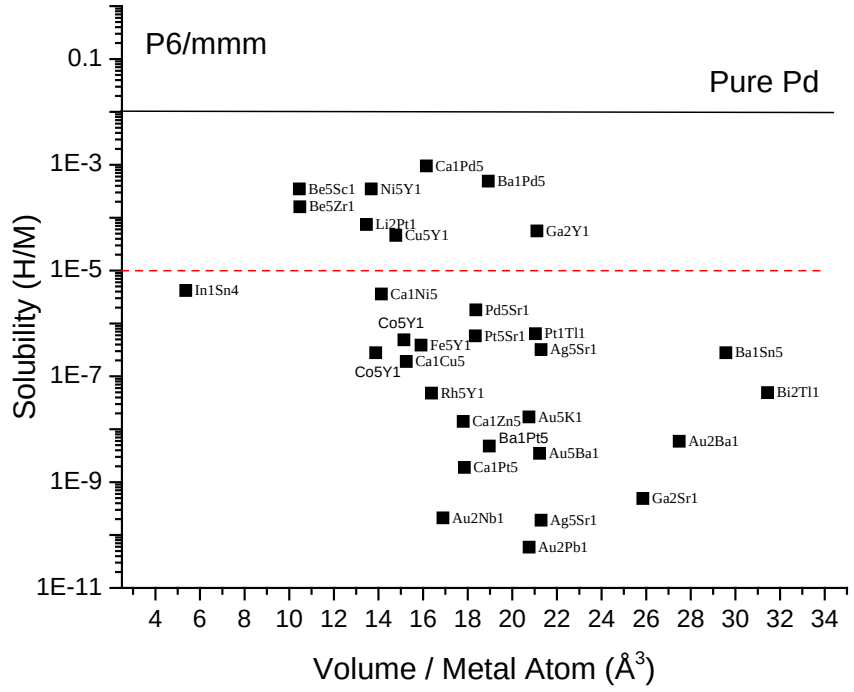
P6/mmm
Pure Pd
Solubility (H/M)
0.1
1E-3
1E-5
1E-7
1E-9
1E-11
4
6
8
10
12
14
16
18
20
22
24
26
28
30
32
34
Volume / Metal Atom (Å3)
Ca1Pd5
Ba1Pd5
Be5Sc1
Ni5Y1
Be5Zr1
Li2Pt1
Cu5Y1
Ga2Y1
In1Sn4
Ca1Ni5
Pd5Sr1
Co5Y1
Pt5Sr1
Pt1Tl1
Fe5Y1
Ag5Sr1
Ba1Sn5
Co5Y1
Ca1Cu5
Rh5Y1
Bi2Tl1
Ca1Zn5
Au5K1
Ba1Pt5
Au2Ba1
Au5Ba1
Ca1Pt5
Ga2Sr1
Au2Nb1
Ag5Sr1
Au2Pb1

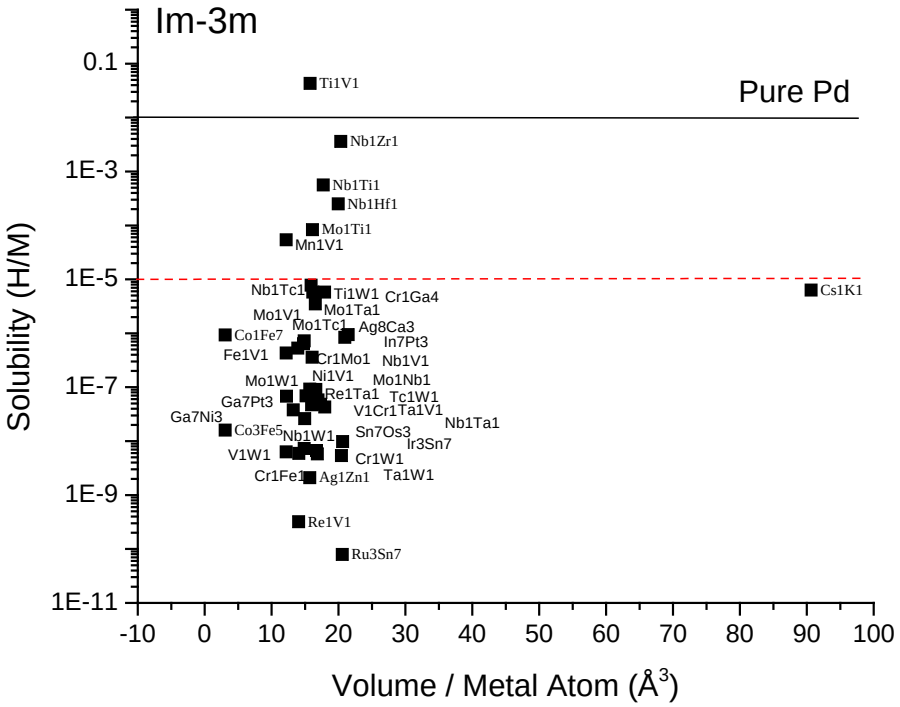
Im-3m
Pure Pd
Solubility (H/M)
0.1
1E-3
1E-5
1E-7
1E-9
1E-11
-10
0
10
20
30
40
50
60
70
80
90
100
Volume / Metal Atom (Å3)
Ti1V1
Nb1Zr1
Nb1Ti1
Nb1Hf1
Mo1Ti1
Mn1V1
Nb1Tc1
Ti1W1
Cr1Ga4
Cs1K1
Mo1Ta1
Mo1V1
Mo1Tc1
Ag8Ca3
Co1Fe7
In7Pt3
Fe1V1
Cr1Mo1
Nb1V1
Ni1V1
Mo1W1
Mo1Nb1
Re1Ta1
Tc1W1
Ga7Pt3
V1Cr1Ta1V1
Ga7Ni3
Nb1Ta1
Co3Fe5
Nb1W1
Sn7Os3
Ir3Sn7
V1W1
Cr1W1
Cr1Fe1
Ag1Zn1
Ta1W1
Re1V1
Ru3Sn7

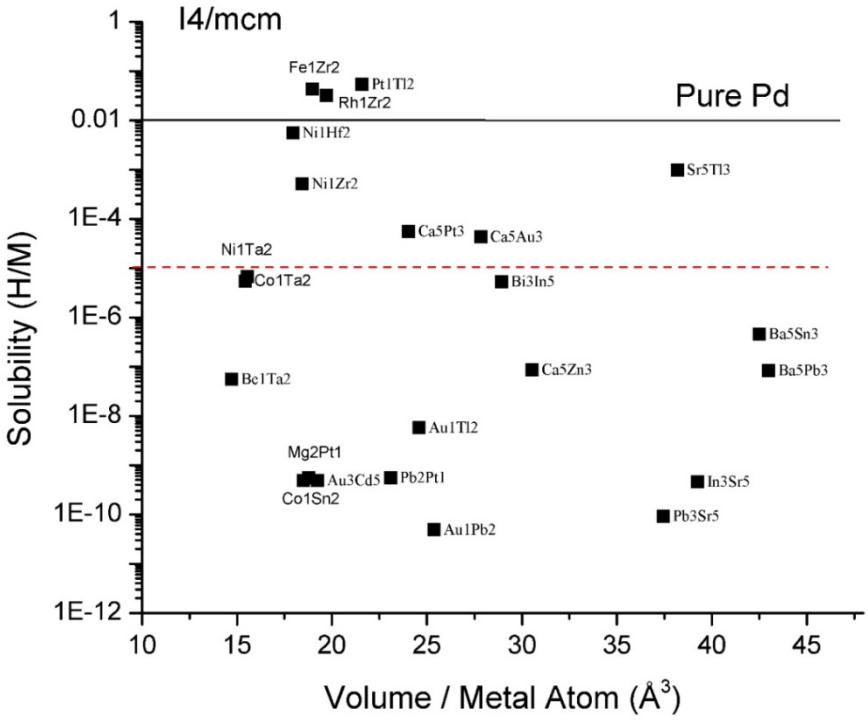
I4/mcm
Pure Pd
Fe1Zr2
Pt1Tl2
Rh1Zr2
Ni1Hf2
Sr5Tl3
Ni1Zr2
Ca5Pt3
Ca5Au3
Ni1Ta2
Co1Ta2
Bi3In5
Ba5Sn3
Ca5Zn3
Ba5Pb3
Bc1Ta2
Au1Tl2
Mg2Pt1
Au3Cd5
Pb2Pt1
In3Sr5
Co1Sn2
Pb3Sr5
Au1Pb2
Solubility (H/M)
Volume / Metal Atom (Å3)

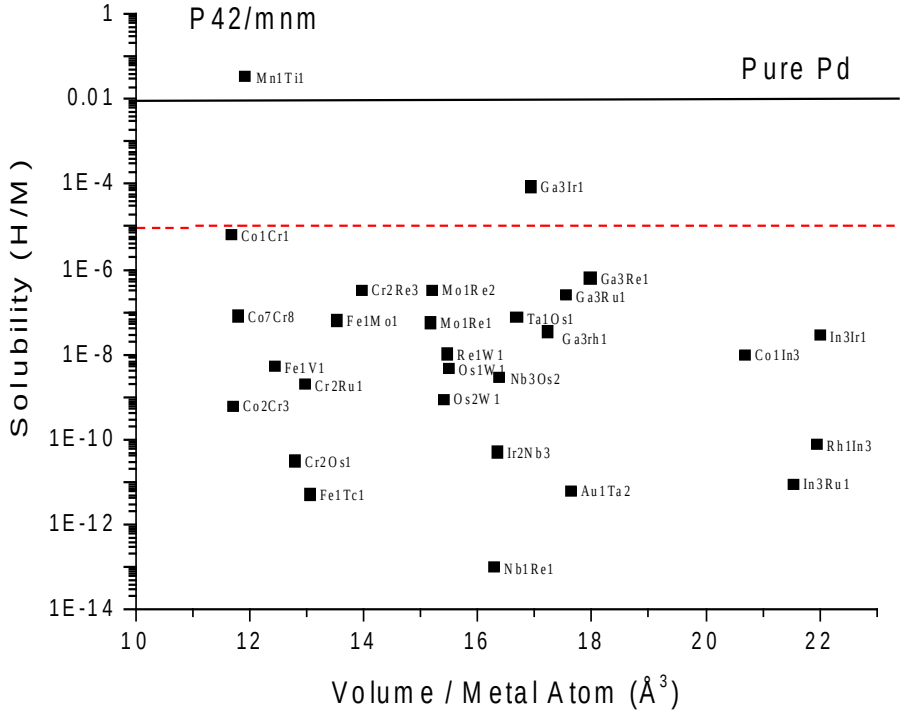
P42/mnm
Pure Pd
Mn1Ti1
Ga3Ir1
Co1Cr1
Ga3Re1
Cr2Re3
Mo1Re2
Ga3Ru1
Co7Cr8
Fe1Mo1
Mo1Re1
Ta1Os1
Ga3rh1
In3Ir1
Re1W1
Co1In3
Fe1V1
Os1W1
Nb3Os2
Cr2Ru1
Co2Cr3
Os2W1
Rh1In3
Ir2Nb3
Cr2Os1
In3Ru1
Au1Ta2
Fe1Tc1
Nb1Re1
Solubility (H/M)
Volume / Metal Atom (Å3)

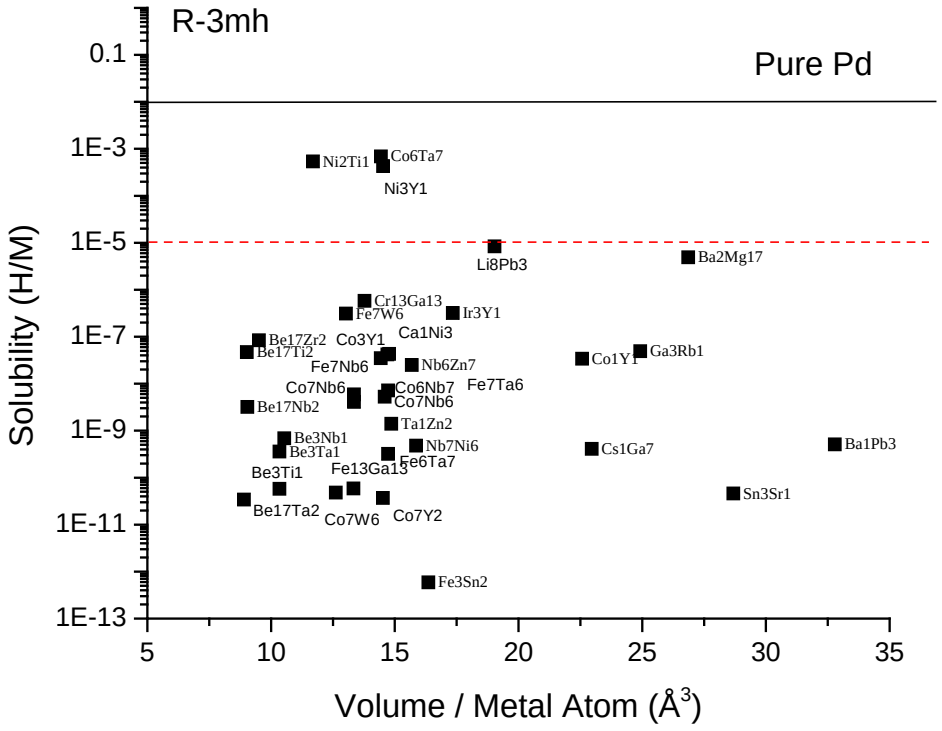
R-3mh
Pure Pd
Solubility (H/M)
Volume / Metal Atom (Å3)
0.1
1E-3
1E-5
1E-7
1E-9
1E-11
1E-13
5
10
15
20
25
30
35
Ni2Ti1
Co6Ta7
Ni3Y1
Li8Pb3
Ba2Mg17
Cr13Ga13
Fe7W6
Ir3Y1
Be17Zr2
Co3Y1
Ca1Ni3
Be17Ti2
Fe7Nb6
Nb6Zn7
Co1Y1
Ga3Rb1
Co7Nb6
Co6Nb7
Fe7Ta6
Co7Nb6
Be17Nb2
Ta1Zn2
Be3Nb1
Be3Ta1
Nb7Ni6
Cs1Ga7
Ba1Pb3
Be3Ti1
Fe13Ga13
Fe6Ta7
Sn3Sr1
Be17Ta2
Co7W6
Co7Y2
Fe3Sn2

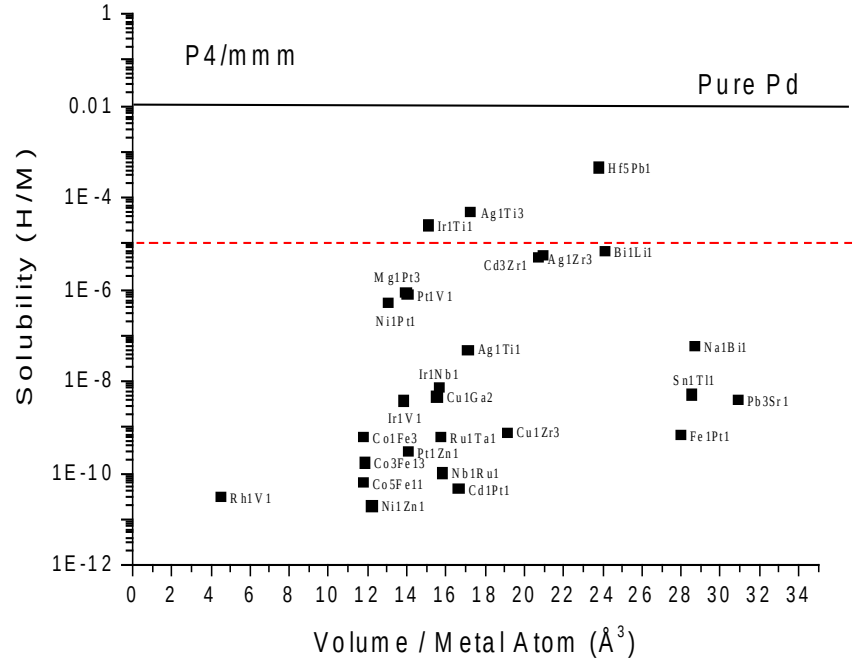
P4/mmm
Pure Pd
Solubility (H/M)
Volume / Metal Atom (Å3)
1
0.01
1E-4
1E-6
1E-8
1E-10
1E-12
0
2
4
6
8
10
12
14
16
18
20
22
24
26
28
30
32
34
Hf5Pb1
Ag1Ti3
Ir1Ti1
Bi1Li1
Cd3Zr1
Ag1Zr3
Mg1Pt3
Pt1V1
Ni1Pt1
Ag1Ti1
Na1Bi1
Ir1Nb1
Sn1Tl1
Cu1Ga2
Pb3Sr1
Ir1V1
Co1Fe3
Ru1Ta1
Cu1Zr3
Fe1Pt1
Pt1Zn1
Co3Fe13
Nb1Ru1
Co5Fe11
Cd1Pt1
Rh1V1
Ni1Zn1

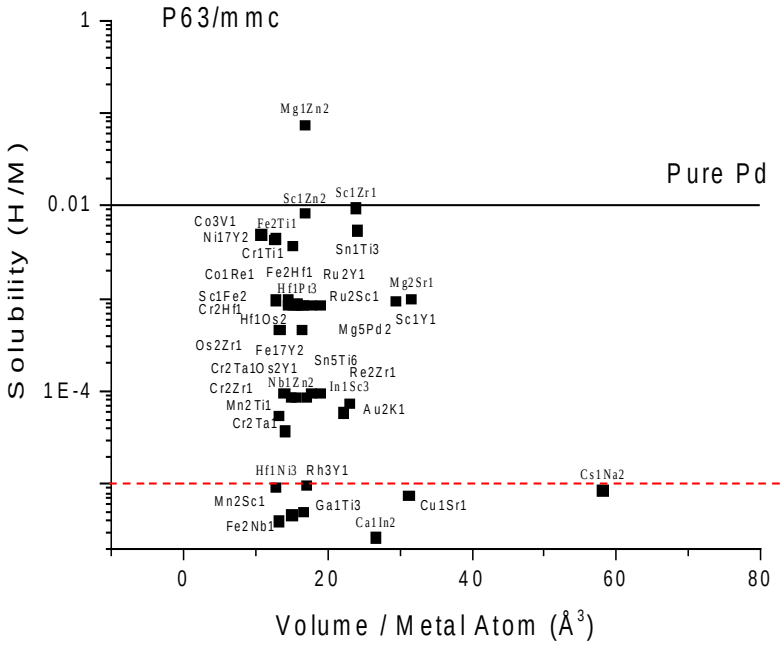
P63/mmc
Pure Pd
Solubility (H/M)
Volume / Metal Atom (Å3)
1
0.01
1E-4
0
20
40
60
80
Mg1Zn2
Sc1Zn2
Sc1Zr1
Co3V1
Fe2Ti1
Ni17Y2
Cr1Ti1
Sn1Ti3
Co1Re1
Fe2Hf1
Ru2Y1
Mg2Sr1
Sc1Fe2
Hf1Pt3
Ru2Sc1
Cr2Hf1
Hf1Os2
Sc1Y1
Mg5Pd2
Os2Zr1
Fe17Y2
Sn5Ti6
Cr2Ta1Os2Y1
Re2Zr1
Cr2Zr1
Nb1Zn2
In1Sc3
Mn2Ti1
Au2K1
Cr2Ta1
Hf1Ni3
Rh3Y1
Cs1Na2
Mn2Sc1
Ga1Ti3
Cu1Sr1
Fe2Nb1
Ca1In2

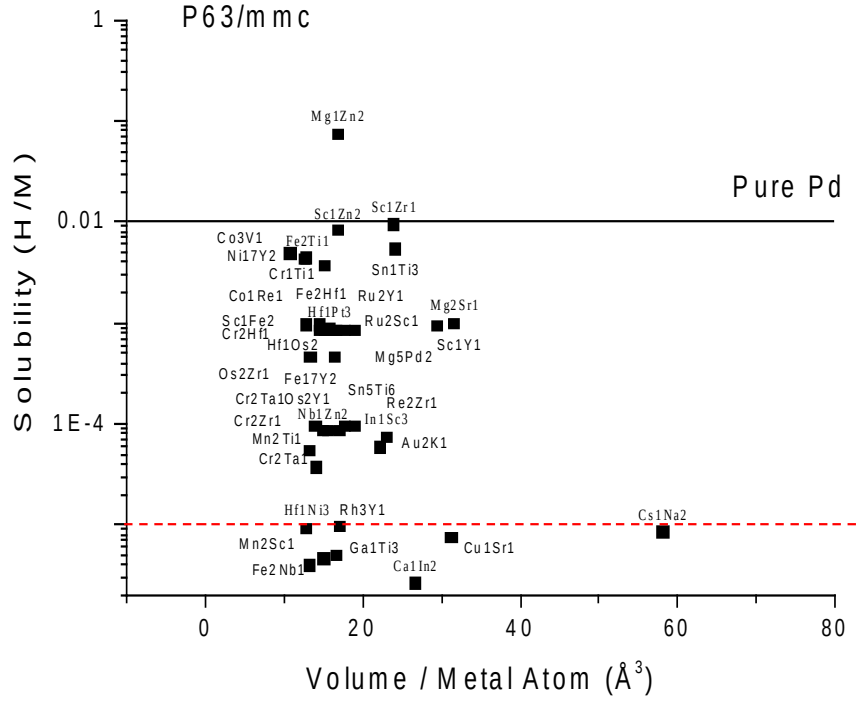
P63/mmc
Pure Pd
Solubility (H/M)
Volume / Metal Atom (Å3)
1
0.01
1E-4
0
20
40
60
80
Mg1Zn2
Sc1Zn2
Sc1Zr1
Co3V1
Fe2Ti1
Ni17Y2
Cr1Ti1
Sn1Ti3
Co1Re1
Fe2Hf1
Ru2Y1
Mg2Sr1
Sc1Fe2
Hf1Pt3
Ru2Sc1
Cr2Hf1
Hf1Os2
Sc1Y1
Mg5Pd2
Os2Zr1
Fe17Y2
Sn5Ti6
Cr2Ta1Os2Y1
Re2Zr1
Cr2Zr1
Nb1Zn2
In1Sc3
Mn2Ti1
Au2K1
Cr2Ta1
Hf1Ni3
Rh3Y1
Cs1Na2
Mn2Sc1
Ga1Ti3
Cu1Sr1
Fe2Nb1
Ca1In2

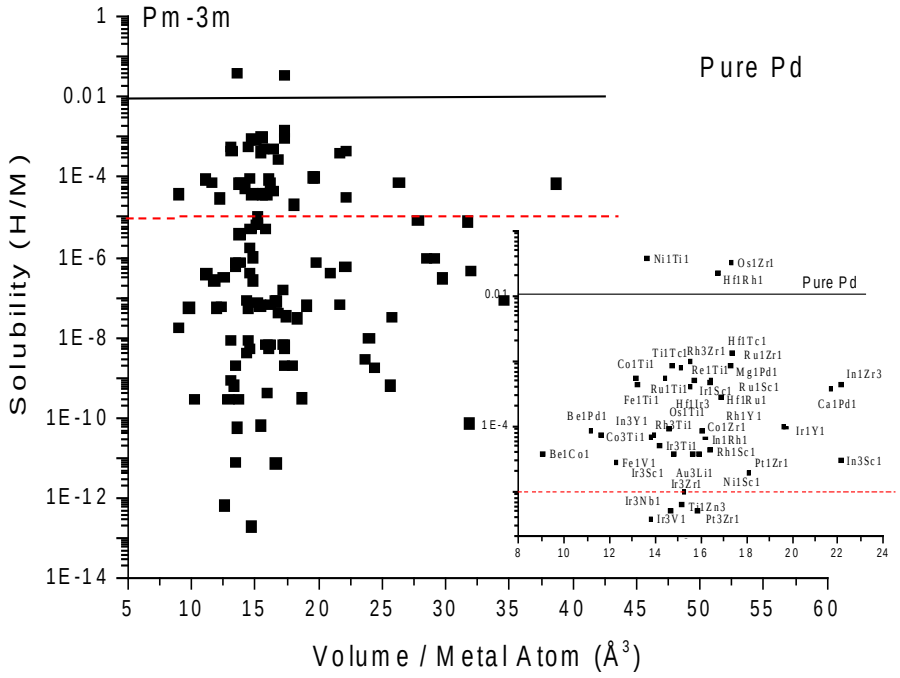
Pm-3m
Pure Pd
Solubility (H/M)
Volume / Metal Atom (Å3)
1
0.01
1E-4
1E-6
1E-8
1E-10
1E-12
1E-14
5
10
15
20
25
30
35
40
45
50
55
60
Ni1Ti1
Os1Zr1
Hf1Rh1
Pure Pd
0.01
1E-4
Hf1Tc1
Ti1Tc1
Rh3Zr1
Ru1Zr1
Co1Ti1
Re1Ti1
Mg1Pd1
In1Zr3
Ru1Ti1
Ir1Sc1
Ru1Sc1
Fe1Ti1
Hf1Ir3
Hf1Ru1
Ca1Pd1
Os1Ti1
Be1Pd1
In3Y1
Rh1Y1
Rh3Ti1
Co1Zr1
Ir1Y1
Co3Ti1
In1Rh1
Ir3Ti1
Be1Co1
Rh1Sc1
Fe1V1
Pt1Zr1
In3Sc1
Ir3Sc1
Au3Li1
Ir3Zr1
Ni1Sc1
Ir3Nb1
Ti1Zn3
Ir3V1
Pt3Zr1
8
10
12
14
16
18
20
22
24

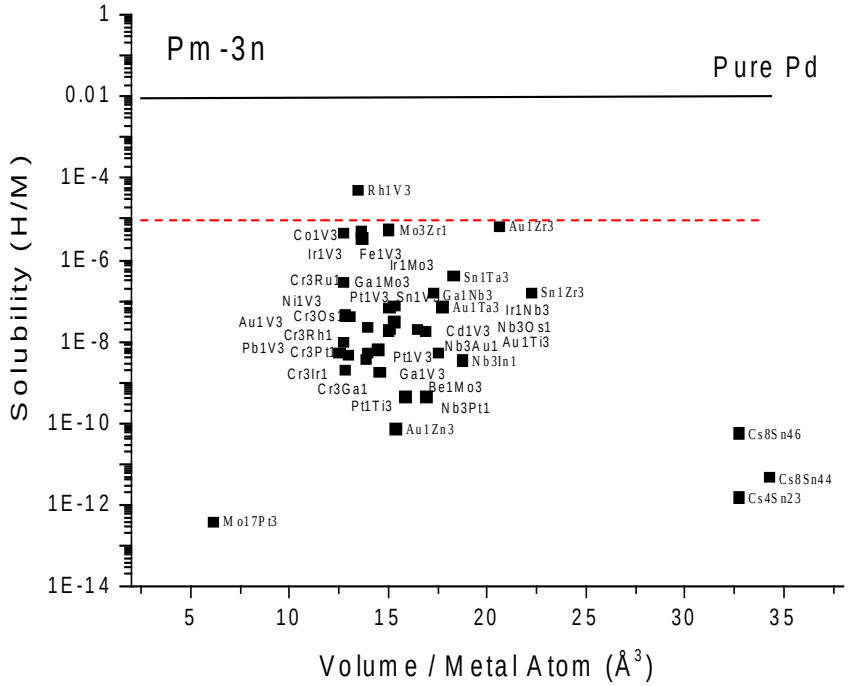
Pm-3n
Pure Pd
Solubility (H/M)
Volume / Metal Atom (Å3)
1
0.01
1E-4
1E-6
1E-8
1E-10
1E-12
1E-14
5
10
15
20
25
30
35
Rh1V3
Mo3Zr1
Au1Zr3
Co1V3
Ir1V3
Fe1V3
Ir1Mo3
Sn1Ta3
Cr3Ru3
Ga1Mo3
Sn1Zr3
Pt1V3
Sn1V3
Ga1Nb3
Ni1V3
Au1Ta3
Ir1Nb3
Cr3Os3
Au1V3
Cd1V3
Nb3Os1
Cr3Rh1
Nb3Au1
Au1Ti3
Pb1V3
Cr3Pt3
Pt1V3
Nb3In1
Cr3Ir1
Ga1V3
Cr3Ga1
Be1Mo3
Pt1Ti3
Nb3Pt1
Au1Zn3
Cs8Sn46
Cs8Sn44
Cs4Sn23
Mo17Pt3

Table S5: Ensemble average binding energies (Eb) and diffusion activation energies (Ea) of shortlisted intermetallics at 600 K and 1 atm H_2. All values are in eV.

Intermetallic	Eb	Ea	Intermetallic	Eb	Ea
Sc1Fe2	-0.07	0.19	Ru2Y1	-0.02	0.39
Rh1V3	0.13	0.21	Ti2Zn1	0.01	0.39
Ni17Y2	-0.12	0.22	Hf5Pb1	0.02	0.39
Pt8V1	0.12	0.22	Pt1Rh1	0.13	0.39
Fe2Y1	-0.22	0.27	Ag1Zr2	0.13	0.39
Mn1V1	0.12	0.23	Cr1Ti1	-0.12	0.4
Mg1Zn2	-0.22	0.27	Be1Pd2	0.01	0.4
Hf1Ta1	-0.13	0.28	Cr1Ti1	-0.13	0.4
Sc1Fe2	-0.07	0.24	Ni3V1	0.13	0.4
Ni2Ti1	0.01	0.25	Ni3V1	0.13	0.4
Fe2Hf1	-0.02	0.26	Rh1Sc1	0.13	0.4
Fe1Ti1	0.02	0.26	Ru2Sc1	-0.02	0.41
Mn1Ti1	-0.19	0.24	Hf5Sn4	0.13	0.41
Hf1V2	0.01	0.27	Ti1Zn16	0.13	0.41
Cs1Au1	0.11	0.27	Pt1Zr1	0.17	0.41
Ru1Zr1	-0.02	0.28	Fe1Zr2	-0.21	0.42
Hf1Mo2	0.01	0.28	Cr2Ti	-0.18	0.42
Sn4Y5	0.10	0.28	Cr2Hf1	-0.02	0.42
Mn2Ti1	0.12	0.28	Nb1Zn2	0.10	0.42
Pb2Y1	0.13	0.28	Tl3Y5	0.10	0.42
Ir1Ti1	0.16	0.28	Ta1V3	0.16	0.42
Pt1Tl2	-0.23	0.29	Rh5Zr3	0.01	0.43
Fe1Hf2	-0.15	0.29	Co1Ti1	0.01	0.43
Nb1Ti1	0.01	0.29	Ta1Ti1	0.01	0.43
Ni3Y1	0.02	0.29	Rh1Y1	0.09	0.43
Hf1Ni1	0.05	0.29	Mo1Ti1	0.10	0.43
Ni1Hf2	-0.14	0.3	Be12Pt1	0.12	0.43
Nb1Zr1	-0.13	0.3	Ir3Y5	0.13	0.43
Pt8V1	0.12	0.3	Rh2Y1	0.13	0.43
Ni2Hf1	0.13	0.3	Sc1Zr1	-0.14	0.44
Co6Ta7	-0.01	0.31	Sn3Y5	-0.05	0.44
Hf1Os2	0.01	0.31	Ni2Sc1	0.00	0.44
Ir1Zr1	0.02	0.32	Li2Pt1	0.10	0.44
Be5Sc1	0.03	0.32	Be12V1	0.12	0.44
Co2Sc1	0.05	0.32	Co2Nb1	0.01	0.45
In3Y1	0.11	0.32	Co2Zr1	0.03	0.45
Cu1Ti2	0.12	0.32	Cr2Ta1	0.09	0.45
Cu5Y1	0.13	0.32	Au2K1	0.12	0.45
Ir1Pt1	0.15	0.32	Ir3Ti1	0.12	0.45
Mg1Pd1	0.01	0.33	Ti1Tc1	-0.02	0.46
Hf5Ir3	0.03	0.33	Ir1Y1	0.09	0.46
Os1Y3	0.10	0.33	In1Rh1	0.11	0.46
Pd2Sr1	0.11	0.33	Ga2Y1	0.12	0.46
Cu1Pt1	0.13	0.33	Os4Zr11	0.13	0.46
Ba1Pd1	0.16	0.33	Ca5Au3	0.13	0.46
Co3V1	-0.12	0.34	Sr5Tl3	-0.02	0.47

Intermetallic	Eb	Ea	Intermetallic	Eb	Ea
Ga3Zr5	0.02	0.34	Ca5Ir1	-0.01	0.47
Ni1Ti1	-0.22	0.30	In1Sc3	0.11	0.47
Os2Zr1	-0.02	0.35	Rh3Ti1	0.11	0.47
Be12Pd1	0.03	0.35	Cr2Ti1	0.13	0.47
Ir2Y1	0.10	0.35	Ca3Pd1	0.14	0.47
Ga3Ir1	0.10	0.35	Cr2Hf1	-0.02	0.48
Ir2Pt1	0.12	0.35	Re1Ti1	-0.01	0.48
Ti1V1	-0.18	0.30	Ir1Sc1	0.01	0.48
Cu1Zr2	-0.05	0.36	Ni2Y1	0.02	0.48
Hf1Pt3	-0.02	0.36	Hf1Ru1	0.04	0.48
Ni1Zr2	0.01	0.36	Sc1Y1	-0.02	0.49
Cd1Zr2	0.01	0.36	Fe17Y2	0.01	0.49
Fe2Zr1	0.01	0.36	In1Zr3	0.02	0.49
Ni1Zr1	0.02	0.36	Ca1Pd1	0.03	0.49
Hf1Mo1	0.03	0.36	Ca5Pt3	0.12	0.5
Ag1Ti3	0.13	0.36	Ca5Pt3	0.12	0.5
In3Sc1	0.15	0.36	Sn3Zr5	0.14	0.5
Cu4Ti3	-0.14	0.367	Ir2Sc1	0.10	0.51
Fe2Ti1	-0.13	0.37	Ag2Sc1	0.09	0.52
Pt2Ta1	0.00	0.37	Hf1Tc1	-0.04	0.53
Ni5Y1	0.03	0.37	Ni1Sc1	0.14	0.53
Nb1Hf1	0.04	0.37	Cr2Zr1	0.10	0.54
Be5Zr1	0.07	0.37	Be1Co1	0.14	0.54
Os2Y1	0.09	0.37	Hf1Ir3	0.02	0.55
Be1Pd1	0.10	0.37	Tl1Y1	0.11	0.55
Sc1Zn2	-0.13	0.38	Co1Zr1	0.10	0.56
Cu1Hf2	-0.12	0.38	Ga3V5	0.12	0.56
Co2Ti1	-0.12	0.38	Mg5Pd2	-0.02	0.57
Mg2Sr1	-0.02	0.38	Sn5Ti6	0.09	0.61
Ru1Sc1	0.01	0.38	Be2Nb1	0.09	0.63
Mo1Zr1	0.02	0.38	Ca1Pd5	-0.02	0.64
Co2Ta1	0.03	0.38	Ru1Ti1	0.01	0.64
Re2Zr1	0.10	0.38	Co3Ti1	0.11	0.64
Cd1Hf2	0.12	0.38	Au41Mg13	0.03	0.65
Ir3Sc1	0.14	0.38	Os1Ti1	0.10	0.66
Rh1Zr2	-0.20	0.39	Au3Li1	0.14	0.67
Co1Re1	-0.02	0.39	Os1Zr1	-0.20	0.78
Rh3Zr1	-0.02	0.39	Sn1Ti3	-0.13	0.86

4. Diffusivity and Solubility normalized to pure Pd of the selected 161 materials.

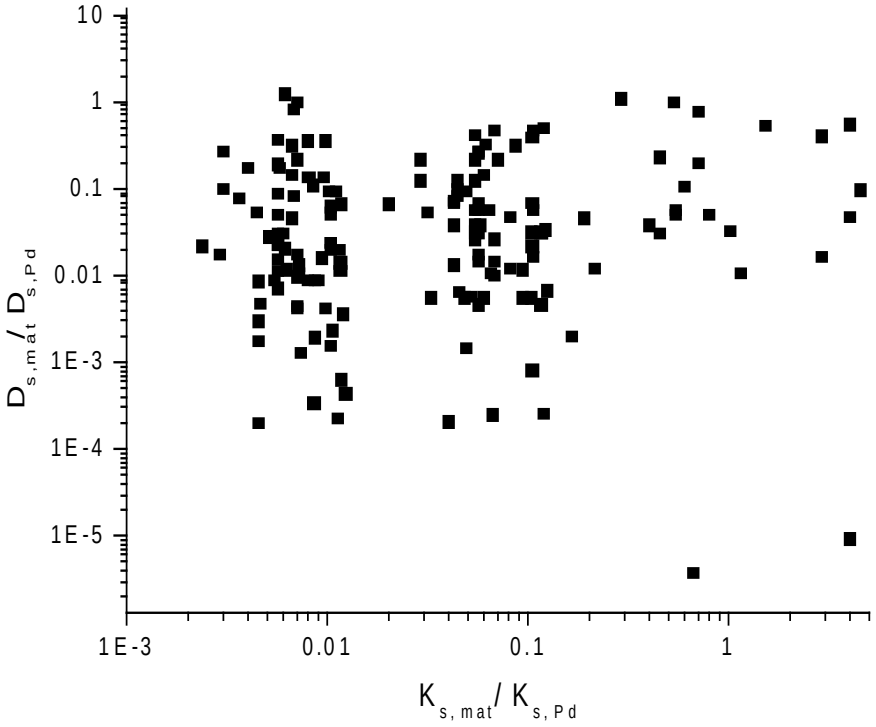

Figure S4: Normalized diffusivity as a function of normalized solubility for 161 intermetallics. The reference system is pure Pd. All properties were calculated at 600 K and 1 atm H_2.

5. Mn-Ti-H equilibrium phase diagram

Using the procedure developed by Alapati and Sholl[6,7] to evaluate the stability of phases for combinations of up to four elements and hydrogen, we predicted the phase diagram of Mn-Ti-H at a H_2 pressure of 1 atm. Figure S4 shows the predicted Mn-Ti-H phase diagram.

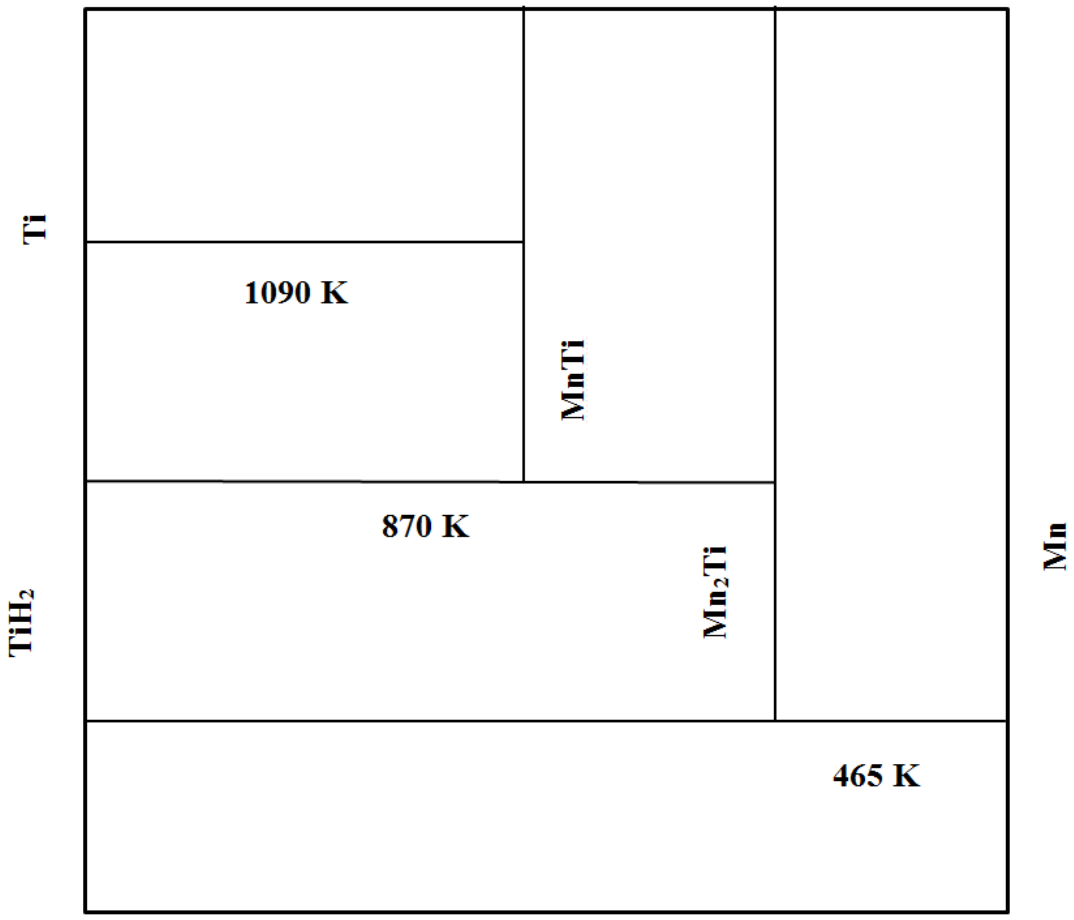

Figure S5: Mn-Ti-H calculated equilibrium phase diagram at 1 atm H_2.The decomposition temperatures of various phases are shown using horizontal lines. The vertical lines indicate the compounds formed. No entropic (vibration effects) were considered in these calculations.

According to our calculations, MnTi is formed at temperatures greater than 870 K. At lower temperatures, MnTi separates to form Mn_2Ti (870-465 K) and further dissociates into the more stable Mn and TiH_2 phases. These calculations were performed at 0 K and do not include vibrational effects. Inclusion of vibrational effects typically lowers the decomposition temperatures but does not qualitatively affect the predicted phase diagram[8-10].

References

1 Kamakoti, P. *et al.* Prediction of hydrogen flux through sulfur-tolerant binary alloy membranes. *Science* **307**, 569-573 (2005).

2 Bergerhoff, G. & Brown, I. D. *Crystallographic Databases*. (International Union of Crystallography, 1987).

3 Ockwig, N. W. & Nenoff, T. M. Membranes for Hydrogen Separation. *Chemical Reviews* **107**, 4078-4110 (2007).

4 Kang, S. G., Coulter, K. E., Gade, S. K., Way, J. D. & Sholl, D. S. Identifying Metal Alloys with High Hydrogen Permeability Using High Throughput Theory and Experimental Testing. *The Journal of Physical Chemistry Letters* **2**, 3040-3044 (2011).

5 Chandrasekhar, N. & Sholl, D. S. Quantitative computational screening of Pd-based intermetallic membranes for hydrogen separation. *J. Membr. Sci.* **453**, 516-524 (2014).

6 Alapati, S. V., Johnson, J. K. & Sholl, D. S. Large-scale screening of metal hydride mixtures for high-capacity hydrogen storage from first-principles calculations. *Journal of Physical Chemistry C* **112**, 5258-5262 (2008).

7 Ozolins, V., Majzoub, E. H. & Wolverton, C. First-Principles Prediction of Thermodynamically Reversible Hydrogen Storage Reactions in the Li-Mg-Ca-B-H System. *Journal of the American Chemical Society* **131**, 230-237 (2008).

8 Nicholson, K. M. & Sholl, D. S. Computationally efficient determination of hydrogen isotope effects on the thermodynamic stability of metal hydrides. *Phys. Rev. B* **86**, 134113 (2012).

9 Nicholson, K. M. & Sholl, D. S. First-Principles Screening of Complex Transition Metal Hydrides for High Temperature Applications. *Inorganic Chemistry* **53**, 11833-11848 (2014).

10 Nicholson, K. M. & Sholl, D. S. First-Principles Prediction of New Complex Transition Metal Hydrides for High Temperature Applications. *Inorganic Chemistry* **53**, 11849-11860 (2014).